CHIN. PHYS. LETT. Vol. 35, No. 6 (2018) 067402

Analysis of the Self-Protection Characteristics of a 1.5 T Bitter-Like HTS Magnet Operated at 65 K *

Yan-Bing Hou(侯言兵), Yin-Shun Wang(王银顺)**, Chang-Tao Kan(阚常涛), Xi Yuan(袁茜), Wei Pi(皮伟)

State Key Laboratory of New Energy Power System, North China Electric Power University, Beijing 102206

(Received 3 January 2018)

We present a conceptual configuration of a high-temperature superconducting (HTS) magnet made from REBCO (Re=Rare Earth, B=Barium, C=Copper, O=Oxide) annular plates, called a Bitter-like HTS magnet, which can operate in persistent current mode without joint resistance and can be excited by a flux pump and without current leads and a persistent power supply. An REBCO annular magnet which can generate 1.5 T corresponding to the operating current density 80% of critical current density of the magnet at an operating temperature of 65 K is conceptually designed. Then the thermal stability of the magnet is numerically simulated by Comsol software. When a piece of REBCO annular plate quenches, the maximum released energy is its stored energy because each REBCO annular plate in the Bitter-like magnet is in parallel. To calculate the stored energy in the REBCO annular plate, the inductance of every annular plate, including self-inductance and mutual inductance, is calculated. Compared with the minimum quench energy (MQE) and stored energy in one REBCO annular plate, the stored energy in one REBCO annular plate is always smaller than the MQE, and the REBCO annular plate will not be damaged even though the stored energy in the REBCO annular plate is fully released, which indicates that this 1.5 T Bitter-like magnet has the property of self-protection.

PACS: 74.25.Fy, 74.72.Bk, 74.78.Bz, 74.81.Bd DOI: 10.1088/0256-307X/35/6/067402

Currently, all commercially available NMR or MRI superconducting magnets are wound by low-temperature superconducting (LTS) wires, such as NbTi and Nb_3Sn conductors. The LTS magnets used in commercial NMR or MRI can operate with persistent current mode (PCM) due to the mature jointing technology. However, an LTS magnet needs liquid helium (LHe) for cooling, which may not be the best option from economic and technical points of view. For devices made by using high-temperature superconducting (HTS) wires, the operating temperature is at 77 K under a lower magnetic field (<1 T) and 30–60 K under a higher magnetic field (3–5 T) and (∼5 K) for ultra-high fields (>15 T).[1] However, so far the jointing technique of HTS wires is not still mature.[2] Compared with conventional LTS magnets in a persistent current switch (PCS), there are a series of difficulties faced by HTS magnets in persistent current mode (PCM), such as high contacting resistance between two HTS wires, and heat leak of current leads.[3]

Quench detection and protection are essential in the operation of HTS magnets. Because most superconducting magnets are now wound with superconducting wires in series,[4–6] all the stored energy of the magnet will concentrate and release in the region of the normal resistive state. The generated heat could lead to severe damage if the heat generated in the resistive part is not promptly removed. Hence, the magnet should be equipped with a sensitive protective system to ensure safe operation of the magnet,[7–9] such a protective system raises the questions of complexity of design and fabrication as well as cost. Therefore, it is of great significance to develop an HTS magnet that has self-protection characteristics.

Figure 1(a) shows the schematic view of an REBCO annular plate with dimensions of each layer. The REBCO annular plate can be obtained by laser-cutting the substrate into circles and then using the mature processes to fabricate other layers. Figure 1(b) is the schematic diagram of the Bitter-like magnet excited by the flux pump. The Bitter-like magnet is alternately stacked by REBCO annular plates and insulation plates. The flux pump is composed of a conventional coil that is at least three times higher than the Bitter-like magnet and an ac power supply which requires that the current rising time is much faster than falling time.

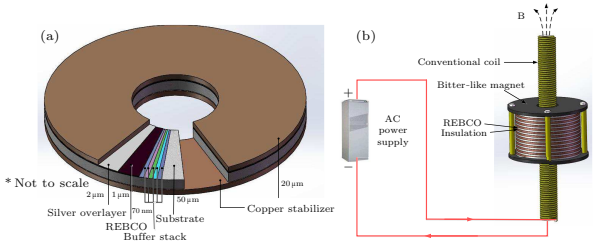

Fig. 1. (a) Schematic view of an REBCO annular plate. (b) Schematic diagram of the Bitter-like magnet excited by the flux pump.

An excitation experiment of the Bitter-like HTS

*Supported by the Fundamental Research Funds for the Central Universities under Grant No 2018MS004.

**Corresponding author. Email: yswang@ncepu.edu.cn

© 2018 Chinese Physical Society and IOP Publishing Ltd

magnet was performed by using a flux pump, which proved the feasibility of this excitation method. The detailed experimental procedure was presented in Ref. [10].

The current density distribution along the radial direction in the REBCO annular plate after excitation is discussed. Considering the axial symmetry, we have the integration form of Maxwell's equation as follows:

$$\oint E \cdot dl = -\iint \frac{\partial B}{\partial t} \cdot dS, \tag{1}$$

where two assumptions are made for simplification: the conventional coil is densely wound by thin wire and the length is infinite, the magnetic field created in the conventional coil is constant, e.g., $B_z = m\mu_0 I$, with m being the turns per meter in the conventional coil.

The other assumption is that the rising rate of the ac power supply is much shorter than the falling rate. That is $\alpha \ll \beta$. Therefore, from Eq. (1) we can derive

$$2\pi \mathrm{r}E \approx -nm\mu_0 \alpha S = -\phi_0, \tag{2}$$

where $r_1 < r < r_2$, r_1 and r_2 represent the inner and outer radii of one REBOC annular plate, respectively, S is the cross-sectional area of the conventional coil, α and β are rising and falling slopes of the ac current, respectively, constant ϕ_0 refers to the induced potential, and n is the number of impulse cycles.

Because the superconductor approximately follows the power law while the current density approaches its critical current density,

$$E = E_\mathrm{c}\left(\frac{J}{J_\mathrm{c}}\right)^n, \tag{3}$$

where J_c represents the critical current density, E_c denotes the electric criterion with 1 μV/cm, and n is the index of the E–J power law.

If the current density approaches the critical current density, based on Eqs. (2) and (3) we can obtain

$$j = J/J_\mathrm{c} = \left(\frac{V_0}{2\pi r E_\mathrm{c}}\right)^{\frac{1}{n}} \propto r^{-\frac{1}{n}}. \tag{4}$$

According to the Bean model, J_c is approximately independent of magnetic field B and r, e.g., J_c is a constant. Figure 2 shows the dependence of the distribution current density on radii at different n values, which shows that the distribution of current density along the radial direction is almost uniform if n is higher than 20.

A Bitter-like magnet that can generate 1.5 T in normal operation state corresponding to the operating current density 80% of critical current density at an operating temperature of 65 K is designed. The inner and outer radii of the REBCO annular plate and insulation plate are 15 mm and 55 mm, respectively.

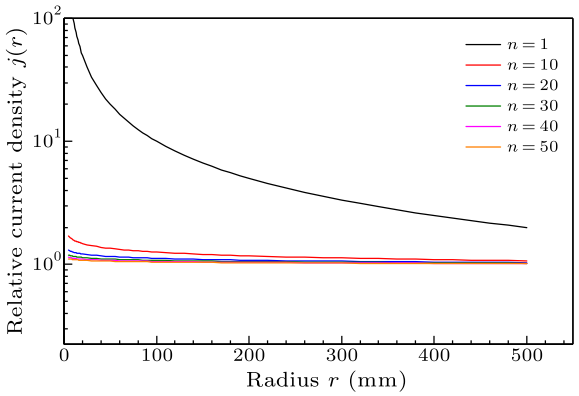

Fig. 2. Relationship of the relative current density with the radius under different n values.

A 2D axial symmetric model was built as shown in Fig. 3 to analyze the magnetic field distribution of the magnet. We found that the magnetic field reaches a maximum on the inner radius of the mid-plane (point A) which is almost perpendicular to the surface of the REBCO annular plate. The closer the two ends of the magnet, the smaller the perpendicular component of the magnetic field is. Thus the critical current density at point A is minimum in the Bitter-like magnet, which is considered to be the maximum current density of the whole magnet. The relationship between the magnetic field and the critical current density is described as[11]

$$J_\mathrm{c}(B) = J_{\mathrm{c}0}\frac{1}{1+B/B_0}, \tag{5}$$

where B is the magnetic flux density, and J_{c0} is J_c for $B = 0$ at 65 K, which is 485 A/mm^2 for engineering current density and $B_0 = 0.5$.

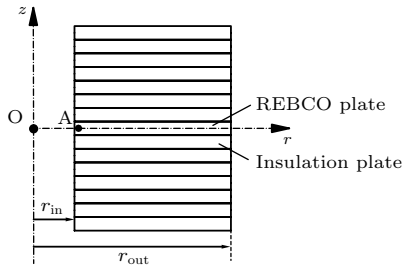

Fig. 3. Schematic diagram of the 2D axial symmetric model.

The dependence of the critical current density on the perpendicular magnetic field and load line at point A is shown in Fig. 4(a). The intersection point P_1 is the critical current density of point A when the number of REBCO annular plates equals 400. The magnetic field generated at point A is 1.93 T, the critical current density $J_\mathrm{c} = 100\,\mathrm{A/mm^2}$, and the magnetic field generated at the central point of O is 1.88 T. During rated operation, the operation current density of the Bitter-like magnet is $0.8J_\mathrm{c}$, with which the magnet can generate 1.5 T at the point of O. The number of REBCO annular plates needed to generate 1.5 T in

rated operation is 400, thus the critical current density of this magnet is 100 A/mm^2.

Because of the high aspect ratio of the REBCO, using the layered structure of the REBCO throughout an entire magnet would be computationally prohibitive, and an homogenized model is adopted to describe the magnet to improve calculation speed and save computation capacity, which has been widely used in dealing with the high aspect ratio of REBCO.[12–14] Consequently, the critical current density of the REBCO annular plate on the inner radius of the mid-plane is the smallest. Therefore, the middle part of the REBCO annular plate in the magnet is the region with the minimum thermal stability. Then a 3D homogenized model was built to study the thermal stability of the middle REBCO annular plate.

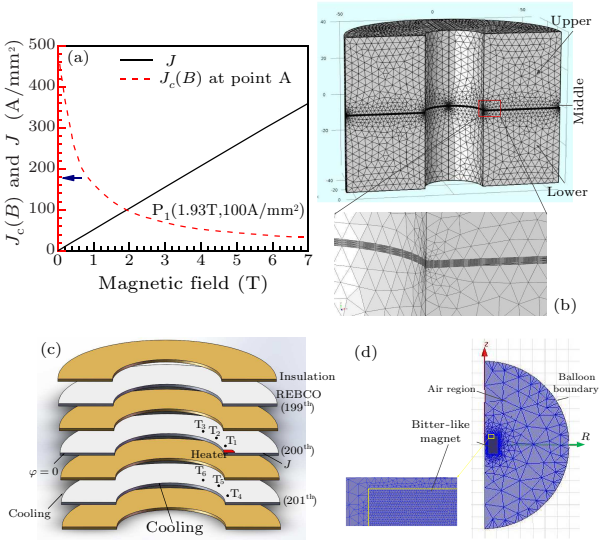

Fig. 4. (a) Dependence of critical current density on perpendicular magnetic field and load line at point A. (b) Meshes of the 3D homogenized model. (c) Schematic view of the middle part in the 3D homogenized model. (d) The 2D axial symmetry model for simulating self-inductance and mutual inductance.

Figure 4(b) illustrates the meshes of the 3D homogenized model which is composed of three parts (upper, middle and lower). In the upper and lower parts, there are 198 and 199 of REBCO annular plates, respectively. In these two parts, the insulation plates are taken into consideration while calculating the homogenized thermal conductivity and electrical conductivity. In the calculation of homogenized thermal conductivity in the azimuthal direction, the insulation plate is neglected due to its low thermal conductivity.

The schematic diagram of the middle part is shown in Fig. 4(c), which consists of three REBCO annular plates (199th to 201st) and four insulation plates. In this model, the current density J is applied on the right side of each REBCO annular plate and the potential φ on the left side is set to be zero. The heater locating in the inner side of the 200th REBCO annular plate is used to trigger the quench. The size of the heater is a fan-shaped area with a radius of 5 mm and an angle of 10°. The temperatures at locations T_1–T_3 on the surface of the 200th REBCO annular plate are calculated to monitor the temperature evolution of the azimuthal direction after heating disturbance is applied. The angles of T_1–T_3 are $\theta = 10°$, $\theta = 30°$, $\theta = 60°$, respectively. In the 201st REBCO annular plate, the temperatures at locations T_4–T_6 in the same angle as the 200th REBCO annular plate are calculated. The periphery of the magnet is cooled by liquid nitrogen and other areas are adiabatic. The dependence of the heat transfer coefficients of liquid nitrogen on temperature difference is obtained from Ref. [15].

The thermal equation for the 3D model is

$$\gamma C\frac{\partial T}{\partial t} - \nabla(k(T)\nabla T) = Q_{\rm j} + Q_{\rm d} - Q_{\rm q}, \qquad (6)$$

where γ is the homogenized mass density, C refers to the homogenized specific heat capacity, T denotes the absolute temperature, k means the homogenized thermal conductivity, $Q_{\rm j} = J\cdot E$ stands for the Joule heat, $Q_{\rm d}$ is the heat disturbance, and $Q_{\rm q}$ is the cooling term.

The electrical conductivity of the superconducting layer including a superconducting and normal conducting components is described by[16]

$$\sigma_{\rm REBCO} = \frac{J}{E_{\rm c}}\left(\frac{J_{\rm c}(B,T)}{J}\right)^n + \sigma_{\rm NC}(T), \qquad (7)$$

where $\sigma_{\rm NC}$ is the electrical conductivity of superconducting layer at normal state, and n is the index of the E–J power law and is set to 28. The dependence of the critical current density on magnetic field and temperature was described in Ref. [11],

$$J_{\rm c}(B,T) = \frac{J_{\rm c0}}{1+B/B_0}\cdot\frac{1-T/T_0}{1-T_0/T_{\rm c}}, \qquad (8)$$

where T_0 is the bath temperature, $J_{\rm c0}$ is the engineering critical current density for the case of $T = 65$ K, and $T_{\rm c}$ is the critical temperature.

The relationship among the stored energy in one REBCO annular plate and self-inductance as well as mutual inductance is

$$W_k = \frac{1}{2}I_k(L_{\rm k}I_k + \sum_{j=1,j\neq k}^{400} M_{kj}\,I_{\rm j}), \qquad (9)$$

where W_k is the stored energy in the kth REBCO annular plate, I_k and $I_{\rm j}$ are separately the currents in kth and jth REBCO annular plates, L_k is the self-inductance of kth plate, and M_{kj} is the mutual inductance between kth and jth plates.

The magneto static method in Ansoft Maxwell software was adopted to calculate the self-inductance and mutual inductance. As shown in Fig. 4(d), a 2D axial symmetry model for simulating inductance is established. The semicircular area is an air region. A

balloon boundary which represents infinity boundary conditions is set in the boundary of air. An excitation current of 1 A is applied in each REBCO annular plate, and every REBCO annular plate is set as 1 turn and is in parallel with other REBCO annular plates.

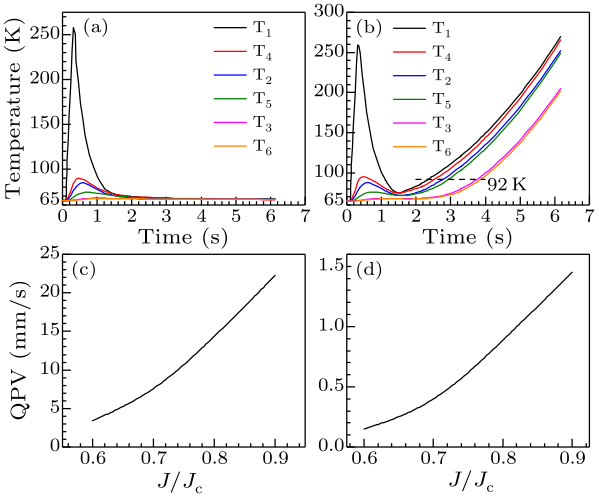

Fig. 5. (a) Temperature evolution of points T_1–T_6 when the applied current density equals 80 A/mm^2 ($0.8J_c$) and Q_d = 0.33 J/mm^2. The applied pulse duration for the heater is 0.25 s. (b) Temperature evolution of points T_1–T_6 with 80 A/mm^2 ($0.8J_c$) and Q_d = 0.34 J/mm^2. (c) Quench propagation velocity (QPV) of azimuthal direction with the normalized current density. (d) QPV of axial direction with the normalized current density.

Figure 5(a) shows the temperature evolution of points T_1–T_6 while the current density J equals 80 A/mm^2 and the applied heat disturbance Q_d is 0.33 J/mm^2. The temperature of point T_1 rises up to 258 K during the heat disturbance and gradually drops to 65 K when the heat disturbance is removed. Figure 5(b) illustrates the temperature evolution of points T_1–T_6 while the current density J equals 80 A/mm^2 and the applied heat disturbance Q_d is 0.34 J/mm^2. The temperatures of points T_1–T_6 continue to rise even when the heat disturbance is removed, which indicated that the REBCO annular plate quenches. In this calculation, the current decay due to the generation of a normal zone is not included and the current is assumed to be constant. The azimuthal quench propagation velocity (QPV) is computed as the distance between T_1 and T_2 divided by the time duration when T_1 and T_2 reach 92 K. The axial QPV is calculated by dividing the distance between T_1 and T_4 and by the time duration when T_1 and T_4 reach 92 K.

Figures 5(c) and 5(d) illustrate the QPV of azimuthal and axial directions with the normalized current density varying from 0.6 to 0.9, respectively. In Fig. 5(c), the QPV of the azimuthal direction changes in the range of 3.38 mm/s–22.3 mm/s with increasing normalized current density from 0.6 to 0.9. In Fig. 5(d), the QPV of the axial direction increases from 0.15 mm/s to 1.45 mm/s corresponding to the normalized current density from 0.6 to 0.9. The QPVs of both azimuthal and axial directions increase with the current density. However, the QPV of the azimuthal direction is much faster than the axial direction. This is mainly due to the anisotropic thermal conductivity of the REBCO annular plate, in which the azimuthal direction is higher than the axial direction. In the axial direction, the thermal conductivity of the insulation plate is also smaller than the thermal conductivity of the azimuthal direction of the REBCO annular plate.

Figure 6(a) indicates the simulating inductance of REBCO annular plates, where only five REBCO annular plates are shown (1st, 100th, 200th, 300th and 400th). The results illustrate that the self-inductance of every REBCO annular plate is the same, that is, 66.8 nH. The mutual inductance between two REBCO annular plates with the same distance is equal.

Figure 6(b) is the sum of self-inductance and mutual inductance of the REBCO annular plate in different positions of the Bitter-like magnet. The results show that the closer to the end of Bitter-like magnet, the smaller the inductance. The inductance of the middle REBCO annular plate (200th) is the largest at 13.12 μH. Hence the stored energy in the 200th REBCO annular plate is the highest.

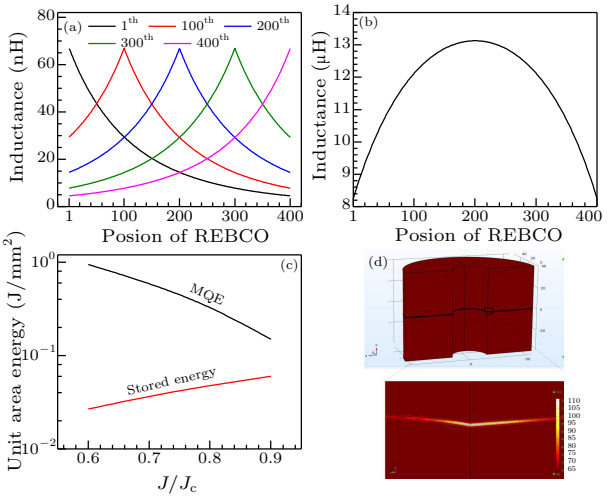

Fig. 6. (a) Inductance of REBCO annular plates in different positions. (b) Sum of self-inductance and mutual inductance of REBCO annular plates in different positions in Bitter-like magnet. (c) MQE and stored energy in the 200th REBCO annular plate. (d) Temperature distribution.

The stored energy and MQE in the 200th REBCO annular plate for the normalized critical current density varying from 0.6 to 0.9 are shown in Fig. 6(c). The stored energy in the 200th REBCO annular plate increases in the range of 0.025 J/mm^2–0.056 J/mm^2 corresponding to the normalized current density of 0.6–0.9, respectively. The MQE of the 200th

REBCO annular plate decreases from 0.95 J/mm^2 to 0.15 J/mm^2 corresponding to the normalized current density of 0.6–0.9. Comparing MQE with stored energy in the 200th REBCO annular plate, the stored energy is always smaller than the MQE during the normalized current density varying from 0.6 to 0.9. As for other positions of REBCO annular plates, the MQE is higher than the MQE of the 200th REBCO annular plate, while the stored energy is less than the energy of the 200th annular plate. Therefore, the stored energy is also smaller than the MQE for REBCO annular plates in other positions.

When a REBCO annular plate quenches, the maximum released energy is its stored energy because each REBCO annular plate in this 1.5 T Bitter-like magnet is in parallel. Figure 6(d) indicates the temperature distribution of the magnet when the stored energy in the 200th REBCO annular plate is fully released in the heater area, where the current density is $0.8J_c$. The maximum temperature in the 200th REBCO annular plate is 111 K, and the maximum temperature in 199th and 201st REBCO annular plates is 71.6 K. It is indicated that the REBCO annular plate will not be damaged even though the stored energy in the REBCO annular plate is fully released, which illustrates that the 1.5 T Bitter-like magnet has the function of self-protection.

In summary, we have presented a Bitter-like magnet excited by a flux pump which can operate in persistent current mode and has the advantage of a compact simple process and being detachable. A 1.5 T Bitter-like magnet consisting of 400 ReBCoO annular plates and operating in 65 K is designed. Comparing the stored energy with the MQE in the 200th REBCO annular plate, the stored energy in the REBCO annular plate is always smaller than its MQE, such that the REBCO annular plate will not be damaged even though the stored energy in one REBCO annular plate is fully released, which indicates that this 1.5 T Bitter-like magnet has the function of self-protection. This characteristic could probably be generalized to other such types of magnets.

References

[1] Obradors X and Puig T 2014 *Supercond. Sci. Technol.* **27** 044003

[2] Ding F Z, Zhang J Y, Tan Y F, Chen Z Y, Dong Z W, Zhang H L, Shang H J, Xu W J, Zhang H, Qu F, Gao Z S, Zhou W W and Gu H W 2018 *Acta Phys. Sin.* **67** 068401 (in Chinese)

[3] Nam S, Lee W S, Lee J, Jeon H, HanS, Choi Y, Lee J and Koe T K 2017 *IEEE Trans. Appl. Supercond.* **27** 4803105

[4] Miyazaki H, Iwai S, Tosaka T, Tasaki K, Hanai S, Urata M, Iokaet S and Ishiial Y 2011 *IEEE Trans. Appl. Supercond.* **21** 2453

[5] Celentano G, Messina G, Angrisani A A, Augieri A, Fabbri F, Galluzzi V, Mancini A, Rizzo F, Rufoloni A, Vannozzi A, Gambardella U, Saggese A and SabatinoP G 2013 *IEEE Trans. Appl. Supercond.* **23** 4600704

[6] Breschi M, Cavallucci L and Ribani P L 2016 *Supercond. Sci. Technol.* **29** 055002

[7] Wakuda T, Ichiki Y and Park M 2012 *IEEE Trans. Appl. Supercond.* **22** 4703404

[8] Fazilleau P, Borgnolutti F and Lécrevisse T 2016 *IEEE Trans. Appl. Supercond.* **26** 4700705

[9] Weijers H W, Markiewicz W D, Voran A J, Gundlach S R, Sheppard W R, Jarvis B and Johnson Z L 2014 *IEEE Trans. Appl. Supercond.* **24** 4301805

[10] Yuan X, Wang Y S, Hou Y B, Kan C T, Cai C B and Sun M J 2018 *IEEE Trans. Appl. Supercond.* **28** 4603005

[11] Berger K, Leveque J, Netter D, Douine B and Rezzoug A 2007 *IEEE Trans. Appl. Supercond.* **17** 3028

[12] Masson P J, Rouault V R, Hoffmann G and Luongo C A 2008 *IEEE Trans. Appl. Supercond.* **18** 1321

[13] Cavaliere V, Masullo G and Formisano A 2009 *IEEE Trans. Appl. Supercond.* **45** 1190

[14] Härö E, Stenvall A, Nugteren J and Kirby G 2015 *IEEE Trans. Appl. Supercond.* **25** 4701505

[15] Roy F, Dutoit B, Grilli F and Sirois F 2008 *IEEE Trans. Appl. Supercond.* **18** 29

[16] Breschi M, Casali M, Cavallucci L, Marzi G D and Tomassetti G 2015 *IEEE Trans. Appl. Supercond.* **25** 4800505